The KOSMA multi-line CO survey of clouds in the Galactic Molecular Ring

Martin Brüll[1], Carsten Kramer[1], Volker Ossenkopf[1,2], Jürgen Stutzki[1], Robert Simon[1], and Frank Bensch[3]

[1] KOSMA, I.Physikalisches Institut, Universität zu Köln, Zülpicher Strasse 77, 50937 Köln, Germany lastname@ph1.uni-koeln.de
[2] SRON National Institute for Space Research, Postbus 800, 9700 AV Groningen, the Netherlands
[3] Harvard-Smithsonian Center for Astrophysics, Cambridge, MA, U.S.A. fbensch@cfa.harvard.edu

1 Introduction

The Milky Way is known to be a spiral barred galaxy with a prominent ring between 4 and 7 kpc Galactocentric radius (Scoville & Solomon 1975; Clemens et al. 1988). Ring resonances occur frequently in barred spiral disk galaxies by gas accumulation under the continuous influence of gravitational torques from the bar pattern. As density enhancements they are often sites of increased star formation (Buta 1999). In an alternative view, this part of our Galaxy can be separated into two spiral arms, the Sagittarius and the Scutum(Cohen et al.1980). The Galactic Molecular Ring (GMR) shows up prominently in CO J=1-0 (Dame et al. 2001) as well as in CI, CII, and NII in the COBE survey (Fixsen et al.1999). Due to its high star formation rate, most of the Galactic giant HII regions, maser sources, and SN remnants are observed towards the ring and most of the Galaxy's FIR luminosity is emitted here (Burton et al. 1976, Bloemen et al. 1990).

2 The KOSMA survey

To study the physical conditions of the molecular gas and their variation within the GMR, we have started a low-J multi-line CO survey of clouds in the GMR with the KOSMA 3m telescope on Gornergrat, Switzerland. This survey complements the Boston University ^{13}CO 1-0 GMR-survey at the FCRAO (Simon et al. 2001; Jackson et al. 2002). At present, we have mapped two fields, a 0.375 deg^2 field at l=45-46 and a 1 deg^2 field at l=30-31 on a fully-sampled grid in CO 3-2, 2-1 and ^{13}CO 2-1 with a velocity resolution of 0.3 km/s. One CO 3-2 channel map corresponding to gas with the velocity of the Scutum arm is shown in Figure 1. The star forming activity is associated with dense and warm molecular clouds traced by the CO 3-2 transition. Both regions contain extended foreground clouds. The GMR material in the G30-31 field is kinematically separated into two regions in the Sagittarius and

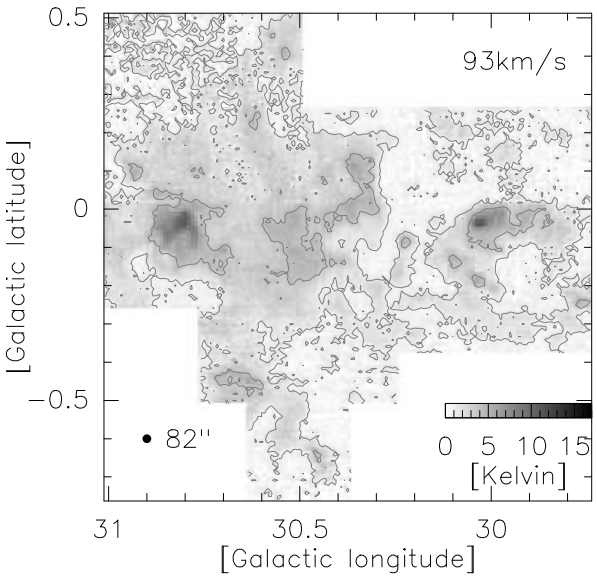

Figure 1: One CO 3-2 channel map of the G30-31 field. The center velocity of 93 km/s corresponds to emission in the Scutum spiral arm. Contours are at 3σ and 10 σ. The field contains the prominent cloud W43, seen at l=30.8, b=-0.1.

Scutum spiral arms, whereas the GMR material in the G45-46 field is only located in the Sagittarius spiral arm.

The data set reveals many different clouds at various Galactic radii. We have started to analyse their properties using radiation transfer models. Here, we are concentrating on studying the observed emission structure.

3 Structure-Analysis

3.1 Cloud structure in different tracers

In the G45-46 field (not displayed here), the foreground source is more fragmented in CO 3-2 than the GMR source which is dominated by large components. To quantify this observation, we used the Δ-variance analysis (Stutzki et al. 1998; Bensch et al. 2001; Ossenkopf et al. 2002) measuring the relative amount of angular structure σ^2(L) of a map depending on the structure size L. This method allows to separate the scaling behaviour of the cloud structure from observational noise and the telescope beam influence (Bensch et al.2001). Figure 2 shows a Δ-variance spectrum of the G45-46 field. The different degree of fragmentation visible in both G45-46 clouds is reflected by different slopes d_Δ in the Δ-variance spectrum (Fig.2). The result for the foreground cloud is nearly equal for the three tracers used for this analysis: d_Δ(CO3-2)=0.65(0.07), d_Δ(CO2-1)=0.63(0.07) & d_Δ(^{13}CO1-0)=0.59(0.05). For the GMR cloud we find: d_Δ(CO2-1)=0.79(0.07), d_Δ(CO3-2)=0.88(0.03) & d_Δ(^{13}CO1-0)=0.98(0.08). Bensch et al. (2001) found for different clouds

a slope of 0.5 $\leq d_\Delta \leq$ 1.3. Our results are in the range of their finding but allows for the first time the comparison of different tracers in equal maps. For all tracers, the slope for the GMR source is higher than for the foreground source, which means that the GMR source is dominated by larger structures. This difference is less obvious in CO 2-1, more pronounced in CO 3-2 and strongest in ^{13}CO 1-0. We explain this finding with widely extended CO 2-1 emission, similar in both clouds. The different slopes in the other tracers then tell us that these, more likely optically thinner lines, reveal different structures for both clouds behind the surface, traced by the CO 2-1 line.

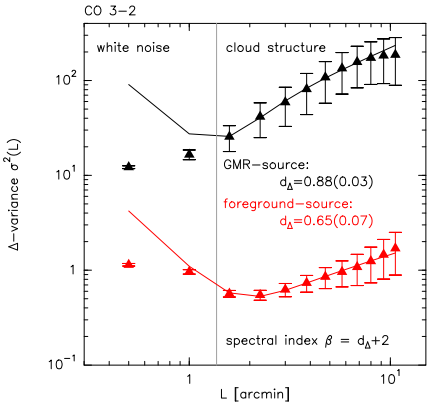

Figure 2: Δ-variance spectrum of the CO 3-2 integrated maps of the G45-46 field as a function of lag-size L. The upper and lower points correspond to the GMR-source (40-80 km/s) and the foreground source (20-30 km/s), respectively. The data are fitted by a power law with radiometric noise and an approximate beam profile. The vertical lines gives the beam-size of 82″. At smaller lags the analytical fit does not work any more. The power law fit is best perfect in the significant range above the beam-size.

3.2 Cloud sizes

Figure 3 shows the application of the Δ-variance analysis to channel maps of the G30-31 field. In many velocity channels the Δ-variance spectrum shows a maximum indicating the maximal angular scale up to which the cloud structure is self similar. At the tangent point (∼105 km/s) we find a typical angular length scale of this maximum of $\sim 10'$, corresponding to 25-30 pc (Fig.3). This scale can be assigned to the size of the dominant structures in the map. We find the same scale size for all tracers, used in this analysis: CO 3-2, CO 2-1 and ^{13}CO 2-1. We call this scale a typical structure or cloud size. Under this assumption, we can solve the distance ambiguity.

Many velocity channels also show a significant amount of structure at sizes larger than the maximum described above. They occur in the velocity channels where OH-, H_2O- and CH_3OH-maser lines were found. Their velocities correspond to the Sagittarius and Scutum spiral arms. We interpret this as the signature of extended diffuse material in the spiral arms. There is no material seen in the interarm regions.

References

1. F. Bensch, J. Stutzki, & V. Ossenkopf A&A **366** 636 (2001)

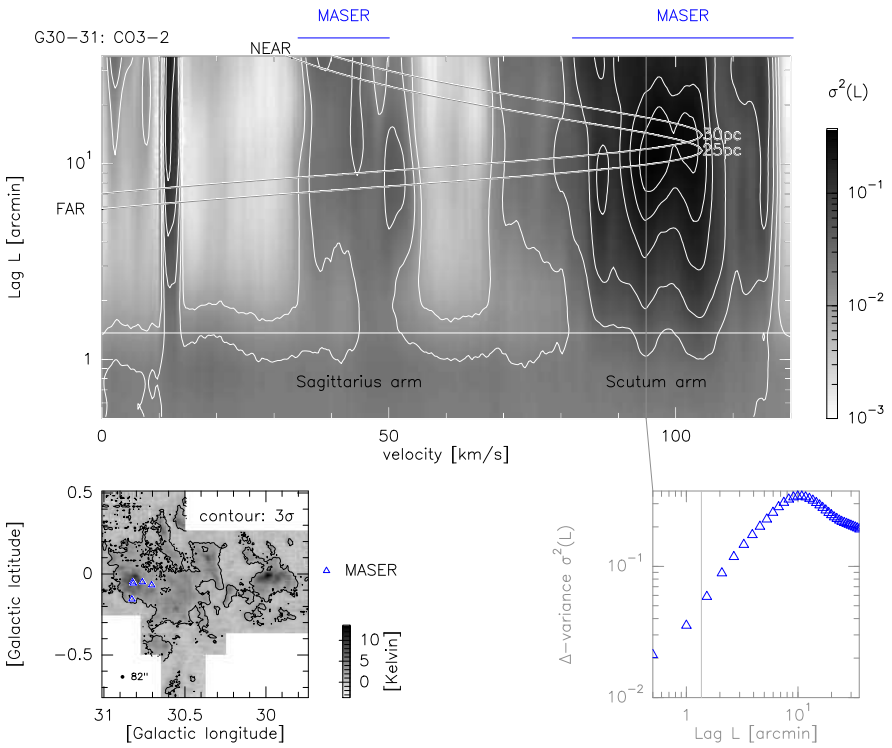

Figure 3: Upper panel: The Δ-variance applied to velocity-channel maps of the G30-31 field in CO 3-2. In the plot of lag-size L versus LSR-velocity, the Δ-variance σ^2(L) is given in grey scales. The horizontal line corresponds to the beam-size. The contours are 2.5, 5, 10, 20, 40, 60 and 80 % of the maximal σ^2(L). The overlayed curves show the scala of 25 and 30 pc assigned by the rotation curve of Wouterloot & Brand (1989); it further illustrates the near/far distance ambiguity. On top the velocity-spread of OH-, H_2O- and CH_3OH-maser lines are shown. **Lower left panel:** One exemplary channelmap at ∼95 km/s. **Lower right panel:** Δ-variance spectrum at this velocity. The vertical line corresponds to the beam-size.

2. J. B. G. M. Bloemen, E. R. Deul, & P. Thaddeus A&A **233** 437 (1990)
3. W. B. Burton ARA&A **14** 275 (1976)
4. R. Buta: AP&SS **269**, 79 (1999)
5. D. P. Clemens, D. B. Sanders, & N. Z. Scoville: ApJ **327**, 139 (1988)
6. R. S. Cohen, et al. ApJ **239**, L53 (1980)
7. T. M. Dame, D. Hartmann, & P. Thaddeus,: ApJ **547**, 792 (2001)
8. D. J. Fixsen, C. L. Bennett, & J. C. Mather ApJ **526** 207 (1999)
9. J. M. Jackson et al. ApJ **566** L81 (2002)
10. V. Ossenkopf, M. Krips, & J. Stutzki A&A submitted (2002)
11. N. Z. Scoville & P. M. Solomon: ApJ **199**, L105 (1975)
12. R. Simon et al. ApJ **551** 747 (2001)
13. J. Stutzki et al. A&A **336** 697 (1998)
14. J. G. A. Wouterloot, & J. Brand A&AS **80** 149 (1989)